Environ. Sci. Technol. **2004**, *38,* 4758−4762

XAS Study of Mercury(II) Ions Trapped in Mercaptan−Functionalized Mesostructured Silicate with a Wormhole Framework Structure

CHIA-CHEN CHEN,[†] EMILY J. MCKIMMY,[‡] THOMAS J. PINNAVAIA,[‡] AND KIM F. HAYES*[,§]

Department of Civil Engineering, University of Texas, Austin, Texas 78712-0273, Department of Chemistry, Michigan State University, East Lansing, Michigan 48824, and Department of Civil and Environmental Engineering, University of Michigan, Ann Arbor, Michigan 48109

Directly assembled wormhole mesostructures with high level functionalized mercaptan (MP-HMS) have been shown to be effective mercury(II) (Hg^{2+}) trapping agents. Sorption of Hg^{2+} onto MP-HMS was investigated using X-ray absorption spectroscopy (XAS) to identify the structural coordination of the adsorbed Hg. Samples with different fractions of mercaptan functionalized groups (i.e., $x = 0.1$ and 0.5) with various Hg/S molar ratios ranging from 0.05 to 1.4 were investigated. XAS analysis indicates that adsorbed Hg first coordination shell is best fitted with an Hg−O path and an Hg−S path. The Hg−S atomic distance (R_{Hg-S}) remained relatively constant while the Hg−S coordination numbers (CN) decreased as Hg/S loading increased. For the Hg−O path, both the CN and the R_{Hg-O} increased with increasing Hg loading. XAS results suggest that at low Hg loadings, adsorbed Hg^{2+} forms mostly monodentate sulfur complexes (−S−Hg−OH) with the sulfur functional groups on the MP-HMS surfaces. At high Hg loadings, the Hg coordination environment is consistent with the formation of a double-layer structure of Hg attached to sulfur binding sites (−S−Hg−O−Hg−OH).

Introduction

Traditional approaches to the removal of mercury ions from solutions have included the use of activated carbon (*1*), zeolites (*2*), silica gel (*3*), sulfide precipitates (*4*), ion-exchange resins (*5, 6*), and clays (*7*) as trapping agents. Low loading capacities and selectivities, and in some cases relatively small metal ion binding constants, have impeded the adoption of these materials for remediation applications. As a "soft" Lewis acid, mercury(II) forms stable complexes preferentially with soft Lewis bases such as mercaptan ligands. Therefore, the selectivity and metal ion binding constants can be vastly improved by attaching chelating mercaptan ligands to a support matrix. An ideal matrix for mercaptan immobilization is one with (i) a high specific surface area for functionalization, (ii) a porous morphology allowing ready access to the sulfur centers, and (iii) a framework structure that is stable under regeneration conditions.

Surfactant templated mesostructures functionalized through reaction with 3-mercaptopropyl trimethoxysilane (MPTMS) have been explored recently as mercury trapping agents. Electrostatic interactions between an ionic surfactant and ionic silica precursors have been utilized to prepare hexagonal MCM-41 (*8*) and SBA-15 (*9*) framework under basic and acidic reaction conditions, respectively. After calcination to remove the surfactant and rehydration so as to generate surface hydroxyl groups, MPTMS is grafted to the framework to yield a functionalized mesostructure (*10*−*12*). In addition to this grafting approach to functionalization, mercaptan ligands can be directly incorporated into the framework structure during the micelle-templated assembly reaction. This yields a structure with the anhydrous formula $(SiO_2)_{1-x}(LSiO_{1.5})_x$, where L is the mercaptopropyl group and x is the fraction of framework sites that are functionalized (*13*).

Recently, high functionalization levels of mercaptan have been directly incorporated into a wormhole mesostructure assembled through hydrogen bonding between a neutral amine surfactant and an uncharged silica precursor. These directly assembled wormhole mesostructures were denoted MP-HMS (*14*). Compositions with x values up to 0.50 were possible. The high mercaptan content along with the wormhole channel motif for facile access to the trapping sites are desirable features of these materials.

An understanding of the bonding sites for mercury in MP-HMS materials may make it possible to improve further the trapping efficiency of these and related mercaptan-functionalized materials. In the present work, we examined by X-ray absorption spectroscopy (XAS) methods the mercury binding sites of MP-HMS. MP-HMS with x values of 0.10 and 0.50 and Hg/S molar ratio in the range of 0.05−1.4 were investigated by both extended X-ray absorption fine structure (EXAFS) and X-ray absorption near edge structure (XANES) analysis.

XAS has been successfully applied in investigations of Hg sorption on various sorbent materials [e.g., activated carbon (*15*), goethite (*16*), microporous SiO_2 (*17*), iron and aluminum oxides (*18, 19*), and pyrite (*20*)]. XAS investigation of Hg−S has also been applied to other types of systems including reduced organic sulfur in humic acid (*21, 22*), thiacrown compounds (*23*), and Hg sulfur interactions in aqueous solutions (*24*). Two recent papers (*10, 25*) by the same research group used XAS to investigate Hg sorption on functionalized monolayers on mesoporous supports similar to the material used in this study. Their findings, however, were inconsistent from one study to the other. The first reported study (*10*) indicated that adsorbed Hg was bonded with one sulfur atom on the solid forming a monolayer while a bridging oxygen was shared with two adjacent Hg atoms. Subsequently, Kemner et al. (*25*) concluded that adsorbed Hg was bonded to two S atoms without any bridging oxygen atom. At issue is the difficulty of determining a unique coordination environment due to the possible multiple scattering paths for Hg−O and Hg−S in the near coordination environment. The inconsistency from the results of previous studies indicates that further XAS studies over a wider range of conditions are necessary to determine the complex Hg−S associations in mesoporous silicate structures.

* Corresponding author telephone: (734)763-9661; e-mail: ford@engin.umich.edu.
[†] University of Texas.
[‡] Michigan State University.
[§] University of Michigan.

10.1021/es049689o CCC: $27.50
Published on Web 08/10/2004

TABLE 1. Experimental Conditions of XAS Samples for MP-HMS $(SiO_2)_{1-x}(LSiO_{1.5})_x$ Compositions with L = Mercaptopropyl and $x = 0.10$ and 0.50

sample id	S fraction (x)	mmol SH/g	mmol Hg added/g MP-HMS	mmol/g Hg sorbed	Hg/S ratio added	Hg/S ratio final	ppm Hg in final solution
X5a	$x = 0.5$	5.28	0.250	0.250	0.05	0.05	<0.02
X5b	$x = 0.5$	5.28	0.494	0.494	0.10	0.10	<0.02
X5c	$x = 0.5$	5.28	3.93	3.83	0.74	0.73	19
X5d	$x = 0.5$	5.28	5.23	5.02	1.0	0.95	42
X5e	$x = 0.5$	5.28	8.55	7.16	1.63	1.36	280
X1a	$x = 0.1$	1.4	0.0615	0.0614	0.05	0.05	0.06
X1b	$x = 0.1$	1.4	0.117	0.117	0.1	0.1	<0.02
X1c	$x = 0.1$	1.4	0.58	0.58	0.5	0.5	<0.02
X1d	$x = 0.1$	1.4	1.15	1.14	0.82	0.81	3.59
X1e	$x = 0.1$	1.4	2.31	1.99	1.65	1.42	144

Experimental Section

MP-HMS Synthesis. Mercaptopropyl functionalized silicas with wormhole framework structures, denoted MP-HMS [with general formula $(SiO_2)_{1-x}(LSiO_{1.5})_x$ where L = mercaptopropyl], were prepared through a previously described direct assembly method (*14*). Typically, 2.2 mmol of dodecylamine surfactant (Aldrich) was dissolved in 2.3 g of ethanol at 65 °C and then diluted with 29 mL of water preheated to 65 °C. The surfactant solution was shaken at 65 °C for 30 min. A 10 mmol quantity of the framework precursors 3-mercaptopropyltrimethoxy silane (MPTMS, Aldrich) and tetraethyl orthosilicate (TEOS, Aldrich) in a x:1−x molar ratio ($x = 0.10$ and 0.50 for this study) was added to the surfactant solution. Each reaction mixture was aged at 65 °C for 72 h. The resulting products were filtered and air-dried for 24 h. The surfactant template was removed from the framework pores by extraction with hot ethanol, and the white MP-HMS products were allowed to air-dry before use. The mercaptan loadings, as determined by ^{29}Si MAS NMR spectroscopy, were 1.4 and 5.2 mmol/g of adsorbent for the products assembled at x values of 0.10 and 0.50. The mercaptan loadings were determined by integrating the T^3 (−69 ppm), Q^3 (−100 ppm), and Q^4 (−110 ppm) resonances associated with the $O_3Si(CH_2)_3SH$ and SiO_4 framework centers, respectively.

Mercury Binding. Samples for EXAFS studies were obtained by adding 200−500 mg quantities of MP-HMS solid in aqueous solutions of mercuric nitrate at an initial mercury concentration of 1000 ppm for 24−48 h. No additional salts or buffers were added to the intrinsically acidic mercury solution. The volume of solution was adjusted to achieve the desired Hg/S ratio. The Hg(II) concentrations of the solutions before and after the addition of MP-HMS were measured by spectrophotometric analysis using diphenylthiocarbazone as the complexant (*26*) with the amount of bound mercury determined by difference. Negligible mercury binding was observed on the silica substrate in the absence of thiol groups.

Characterization of Mercury Binding. The ^{29}Si MAS NMR spectra used to determine the mercaptan loadings were collected on a Varian 400 solid-state NMR spectrometer with field strength of 400 MHz, under single-pulse mode with a zirconia rotor at a spinning frequency of 4 kHz. A pulse delay of 400 s was employed so that there was sufficient time for the nuclei to relax before application of another pulse. Talcum powder was used as a reference.

Mercury EXAFS Analysis. Samples for XAS studies were prepared by equilibrating the adsorbents with solutions of different Hg concentrations for 24 h as described above. The slurries were then filtered, and the solid phase was either allowed to dry in air or was stored as a fresh paste for XAS experiments. The experimental conditions of the adsorption samples are listed in Table 1. To test whether air-dried process would alter the adsorbed Hg coordination structure, two sets of samples were prepared under same experimental conditions with one set in a paste form and the other as an air-dried solid. These two sets of samples covered most of the experimental conditions for the samples collected in the XAS experiments. From the XANES spectra and EXAFS analysis of these samples, it was found that the air-drying did not alter Hg coordination parameters. These data also indicate that Hg entrained in the fluid in wet pastes does not influence the sorbed Hg coordination analysis.

Several XAS spectra of Hg model compounds were collected to compare with the spectra from Hg adsorbed samples. Cinnabar and metacinnabar were selected to provide models of octahedral and tetrahedral Hg−S coordination, respectively. HgCl and $HgCl_2$ were used for evaluating the oxidation state of sorbed Hg through XANES analysis. HgO and Hg(II) aqueous samples were chosen to evaluate sorbed Hg in comparison to precipitated and hydrated aqueous Hg−O structure. The Hg(II) aqueous sample was prepared by dissolving mercury nitrate salt in water to make a final Hg solution with concentration of 0.141 M while HgO(s) was used as received.

X-ray absorption spectra were collected at the Hg L3-edge at beamline 4-1 or 4-3 in the Stanford Synchrotron Radiation Laboratory (SSRL) using Si(220) monochromators. The spectra were collected in fluorescence mode at room temperature using a 13-element Ge detector. XAS data were analyzed using the computer program EXAFSPAK (*27*). XAS raw spectra were normalized using a Victorian function and spline fitted to extract EXAFS signals. Structural information for the sorption complexes was then determined by fitting the unknown spectra with nonlinear least-squares methods using phase and amplitude parameters obtained from theoretical calculation results of FEFF8.0 (*28*) without any filtering. Least-squares fitting of each shell results in the determination of the coordination number (CN) and the bonding distance (R). The Debye−Waller factor (σ^2) and ΔE_o (E_o is defined as the energy at which $k = 0$), were allowed to vary during the optimization of CN and R. In fitting multiple paths (detailed description is discussed below), σ^2 was subsequently fixed while ΔE_o was allowed to vary. Once optimized, σ^2 was then kept the same for the multiple path analysis. The resulting CN and R, based on this fitting procedure, are expected to be accurate to ±10% and ±0.02 Å, respectively, for the first shell when single absorber−scatterer paths are fit (*29*). XANES analysis was performed by qualitative comparison of the shapes and position of the edge region of the XAS spectrum.

Results and Discussion

X-ray Absorption Near Edge Structure (XANES). XANES data for Hg model compounds and samples of MP-HMS $(SiO_2)_{1-x}(LSiO_{1.5})_x$ compositions with $x = 0.1$ and 0.5 and various Hg/S loading levels were extracted from the raw XAS spectra and normalized to the absorbance at the peak of the edge jump (Figures 1 and 2). XANES spectra, in general, are primarily sensitive to the first shell coordination structure and provide qualitative information about changing structural characteristics based on differences in observed XANES features. The collected XANES spectra of cinnabar and metacinnabar clearly show structural differences in the first shell as evidenced by the different spectral features (as indicated by the arrows in Figure 1). Similarly, changes in sorbed Hg coordination structure as a function of Hg/S loadings can be observed from their XANES spectra.

XANES can often be used to determine the oxidation state of a given element by observing the energy shift of the absorption edge. For Hg, however, the energy shift for HgCl and $HgCl_2$ model compounds were not significantly different. In fact, the XANES of these two compounds actually crossed

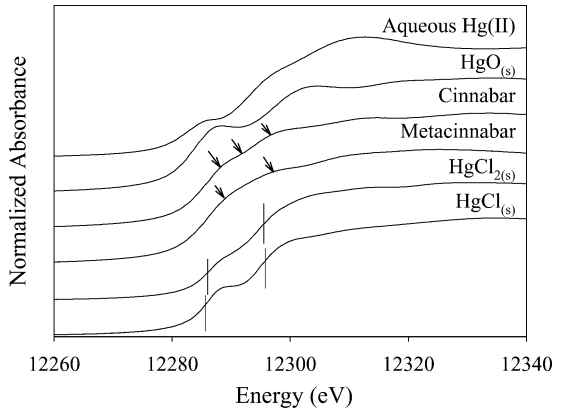

FIGURE 1. XANES spectra of Hg model compounds. The arrows indicate the difference between XANES features of cinnabar and metacinnabar. The vertical bars indicate the difference of the inflection points between Hg with different oxidation states.

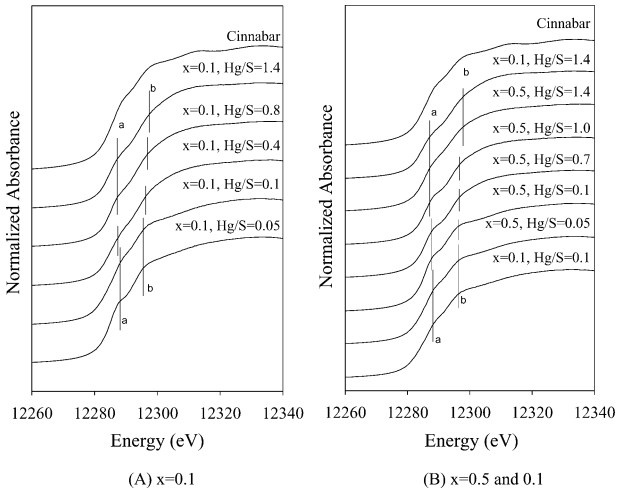

FIGURE 2. XANES spectra of Cinnabar and MP-HMS $(SiO_2)_{1-x}(LSiO_{1.5})_x$ mesostructures where L = mercaptopropyl, with (A) $x = 0.1$; (B) $x = 0.5$ and 0.1, and various Hg/S loading levels. The vertical bars denote the differences of features "a" and "b"among different samples.

each other with the largest energy shift observed of about 1 eV around the first inflection point of the edge jump (indicated by the vertical bars in Figure 1). Theoretical FEFF8.0 calculations of the XANES spectra for $HgSO_4$ and Hg_2SO_4 also showed only slight differences in the position of the edge. Therefore, inferring Hg(II) oxidation state changes by XANES analysis for Hg is difficult. Nevertheless, since our samples, which were prepared under ambient conditions and exposed to an oxidizing environment, did not show even a hint of an energy shift of edge position among all the sorption samples, we conclude that the Hg(II) retained its oxidation state in this study.

As seen in Figure 2A, for functionalized MP-HMS with $x = 0.10$, the XANES spectra were similar for Hg/S < 0.10, suggesting that adsorbed Hg maintained similar near coordination structure at these comparatively low mercury Hg^{2+} loadings. When Hg^{2+} loading was increased, however, the coordination structure of adsorbed Hg changed accordingly as evidenced by the increasing spacing between XANES features "a" and "b". XANES spectra of samples with $x = 0.50$ showed spectral trends similar to those of the $x = 0.10$ samples insofar as the spacing between XANES features a and b increased with increasing Hg/S loadings (Figure 2B). It should be noted that the XANES spectra of samples $x = 0.1$, Hg/S = 0.1 and $x = 0.5$, Hg/S = 0.05 are very similar to each other. However, the XANES spectra of $x = 0.5$ changed noticeably

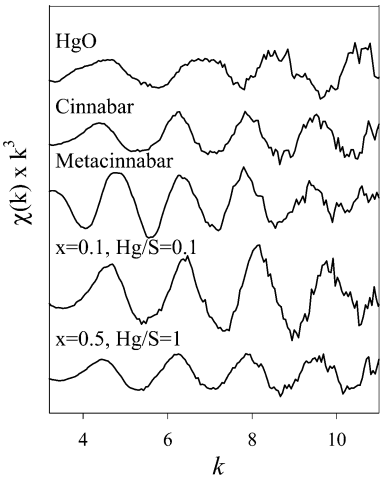

FIGURE 3. EXAFS spectra of MP-HMS $(SiO_2)_{1-x}(LSiO_{1.5})_x$ mesostructures with L = mercaptopropyl, $x = 0.1$ and 0.5, and various Hg/S loading levels.

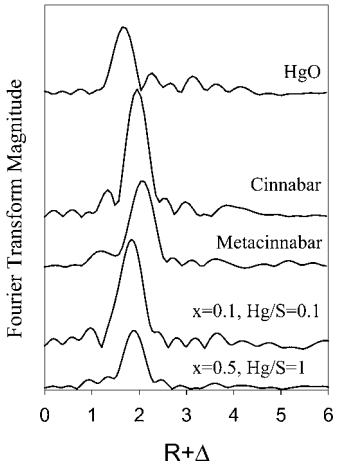

FIGURE 4. RDFs of MP-HMS $(SiO_2)_{1-x}(LSiO_{1.5})_x$ mesostructures with L = mercaptopropyl, $x = 0.1$ and 0.5, and various Hg/S loading levels.

from the lowest coverage of Hg/S of 0.05 to 0.1 while XANES spectra of Hg/S = 0.05 and 0.1 for $x = 0.1$ samples showed very similar XANES features. This result indicates that the proportion of sulfur functionalized sites (x) and the Hg/S loading can affect the coordination structure of adsorbed Hg, with the loading affect particularly noticeable at the higher extent of surface functionalization. This may be due to a saturation of functionalized surface sites at lower loadings for $x = 0.1$ compared to the $x = 0.5$ systems over the range of loadings investigated. From the XANES spectra alone, however, it is not possible to be more definitive about the cause of the functionalization extent on the near coordination environment.

For samples with highest Hg/S loadings, where the number of sulfur functionalized sites were less than the amount of sorbed Hg (i.e., Hg/S > 1), the XANES spectra between samples of $x = 0.1$ and $x = 0.5$ were almost identical to each other. This observation suggested that Hg coordination structure is not affected by the proportion of the sulfur functionalized sites at these over saturation Hg/S loading levels. This, however, does not rule out the possibility that monolayer saturation of sulfur functionalized surface sites can occur at lower Hg/S < 1 loadings as suggested by the $x = 0.1$ data.

Extended X-ray Absorption Fine Structure (EXAFS). Figures 3 and 4 show the EXAFS spectra and radial distribution functions (RDFs), respectively, for the selected Hg model

TABLE 2. Best Fits of EXAFS Results for MP-HMS $(SiO_2)_{1-x}(LSiO_{1.5})_x$ Compositions with L = Mercaptopropyl and $x = 0.10$ and 0.50

	S fraction		Hg−O			Hg−S		
sample	(x)	Hg/S	CN	R	σ^2	CN	R	σ^2
X5a	0.5	0.05	1.2	2.18	0.003	1.1	2.38	0.0022
X5b	0.5	0.1	1.6	2.22	0.003	1.1	2.38	0.0022
X5c	0.5	0.7	1.7	2.26	0.003	0.5	2.39	0.0022
X5d	0.5	1.0	1.9	2.29	0.003	0.6	2.40	0.0022
X5e	0.5	1.4	1.9	2.30	0.003	0.6	2.39	0.0022
X1a	0.1	0.05	1.2	2.18	0.003	1.0	2.38	0.0022
X1b	0.1	0.1	1.2	2.16	0.003	1.1	2.39	0.0022
X1c	0.1	0.4	1.7	2.23	0.003	0.7	2.40	0.0022
X1d	0.1	0.8	1.8	2.27	0.003	0.7	2.41	0.0022
X1e	0.1	1.4	1.9	2.29	0.003	0.7	2.40	0.0022

	Hg−O		
	CN	R	σ^2
α-HgO(s)	2.5	2.05	0.004
aqueous Hg(II)	2.2	2.30	0.012

	Hg−S			Hg−S		
	CN	R	σ^2	CN	R	σ^2
cinnabar	2.0	2.38	0.0035	0.5	3.33	0.0037
cinnabar-XRD[a]	2.0	2.36		2.0	3.30	
metacinnabar	3.1	2.25	0.0095			
metacinnabar-XRD[b]	4.0	2.53				

[a] Based on data from ref *30*. [b] Based on data from ref *31*.

compounds and Hg sorption samples for $x = 0.1$ and 0.5. The RDFs were derived by Fourier transform of EXAFS spectra in the k range from 3.5 to 11. Since EXAFS spectra and RDFs show little differences among the adsorption samples, only one sample spectrum from each set of samples with different mercaptan substitution (i.e., $x = 0.1$ and 0.5) is shown on the graphs. Sample conditions and fitted results from EXAFS analysis are listed in Table 2.

Each mercury-loaded MP-HMS as well as both cinnabar and metacinnabar model compounds exhibit only one significant RDF peak. Even though the model compounds are well crystallized, no other noteworthy peaks are found in the RDFs. This is uncommon for EXAFS spectra for most elements in well crystallized environments. The attenuation of second shell RDF peaks, however, is consistent with previously published Hg XAS work on HgO and HgS model compounds (*22*). EXAFS analysis of the first shell of the model compounds matches the coordination structure parameters derived form crystallography data obtained from XRD analysis (Table 2). The second shell coordination information from EXAFS spectra is either missing (metacinnabar) or significantly underestimated (cinnabar) compared to crystallography results. The lack of accurate estimation of the second and subsequent coordination shells restricts the data analysis of Hg EXAFS spectra to the nearest neighboring atoms only. This result is not due to a poor signal to noise ratio but is a characteristic of Hg L3 spectra for all samples analyzed in this work. Spectra of all the Hg sorption samples show only one significant first shell RDF peak, similar to the model compounds, as has also been noted previously (*20*, *22*−*24*).

Several approaches were used to fit the EXAFS spectra. Intuitively, one would expect that adsorbed Hg would form either monodentate or bidentate complexes with sulfur atoms of mercaptopropyl functionalized surface reaction sites depending on their proximity to one another. Given that aqueous Hg(II) has two oxygens in the first shell prior to sorption (Table 2), the expectation is that upon sorption the first shell will possibly contain one Hg−S path and one Hg−O path (for monodentate sulfur complexes), or one Hg−S path

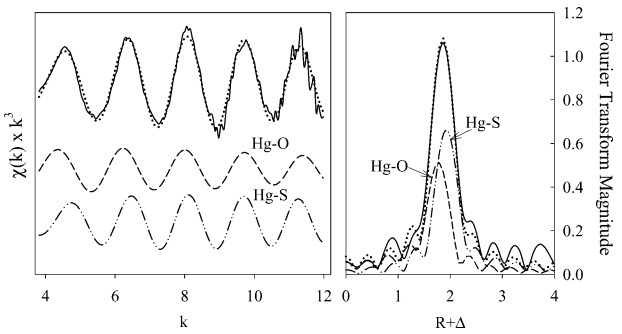

FIGURE 5. EXAFS spectrum and RDF of adsorption sample $x = 0.5$ and Hg/S = 0.1 showing experimental data and fit result (solid line: experimental data; dotted line: fit data; dashed line: component from Hg−O path; dashed-dotted line: component from Hg−S path).

only (for bidentate sulfur complexes), or a combination of both types of complexes. The data analysis showed no statistical difference in the goodness of the fit from assuming a combination of one Hg−S and one Hg−O path versus only one Hg−S path. Using the Hg−S path alone resulted in unrealistically large ΔE_o values (>30 eV), suggesting that one Hg−S path cannot fit the EXAFS spectra. It is possible that a S−Hg−S bidentate structure might contain two different Hg−S atomic distances. EXAFS analysis, however, will not distinguish two Hg−S distances in the first shell unless the difference between these two distances is large enough (e.g., larger than 0.1 Å based on FEFF calculations), since EXAFS only gives average structural information. Fitting the results to two Hg−S paths resulted in a large ΔE_o value (>30 eV) without any improvement in the goodness-of-fit. Previous EXAFS analysis on Hg adsorbed onto FeS (*20*) or for sulfur in humic acid (*22*) resulted in a Hg−S atomic distance similar to the one reported here (Table 2), suggesting that the approach adapted in this work of using one Hg−S and one Hg−O path in the first shell analysis is reasonable and the most logical given the data fitting constraints.

During the fitting routine of the first shell using the two paths, the Debye−Waller factor was initially used as an adjustable parameter to get the best fit. The Debye−Waller factors (σ^2) so obtained were within a narrow range among the adsorption samples: from 0.00282 to 0.00308 for Hg−O paths and from 0.00202 to 0.00230 for Hg−S paths. It should be pointed out that the structural parameters (especially coordination numbers) deduced from the fitting of these two paths were very sensitive to a minor change of Debye−Waller factor. Therefore, to compare the results from different samples in a self-consistent way, the Debye−Waller factor was fixed at 0.003 for Hg−O and at 0.0022 for Hg−S. These values were chosen based on the median value of all samples rather than the mean as this was considered the most representative. The goodness of fit for the EXAFS spectrum of adsorption sample with $x = 0.1$, Hg/S = 0.8 using the approach described above is shown in Figure 5.

The results from the EXAFS analysis procedure showed a general trend for samples with functionalized compositions of $x = 0.1$ and 0.5 (Table 2). The Hg−S atomic distance (R_{Hg-S}) remained relatively constant while the Hg−S coordination numbers (CN) decreased as Hg/S loading increased. For the Hg−O path, both the CN and the R_{Hg-O} increased with increasing Hg loading. In fitting the first shell paths using one absorber-scatterer pair, as mentioned in the experimental methods section, errors of ±10% and ±0.02 Å are expected for the average CN and bond distance, respectively. It should be noted, however, that a systematic error in CN and bonding distances may result when two paths are used to fit a single shell due to the interdependence of CN and bonding distance on the relative contributions of Hg−S and Hg−O path. This may lead to potentially larger errors than single shell fits

using one path.

EXAFS analysis for MP-HMS samples of $x = 0.1$ and 0.5 with lowest Hg/S loading (i.e., Hg/S = 0.05), results in the Hg−O shell with a coordination of CN = 1.2 ± 0.2 and R_{Hg-O} = 2.18 ± 0.02 Å and the Hg−S shell with a CN of 1.0 ± 0.2 and R_{Hg-S} = 2.38 ± 0.02 Å. When the Hg/S loading increases to 0.1, the Hg−O coordination parameters remain relatively the same for the $x = 0.1$ sample. The Hg−O coordination parameters of the $x = 0.5$ sample, however, increase with CN = 1.6 and R_{Hg-O} = 2.22 ± 0.2 Å. The CN and atomic distances between Hg and S remain the same (CN = 1.1, R = 2.38 Å) for both systems. These changes in the near coordination environment with coverage for different sulfur functionalization extents are consistent with the findings from XANES analysis as discussed above.

The Hg−S distance is consistent with Hg adsorbed as a monodentate sulfur complex on sulfur functional sites while the Hg−O distance is consistent with that of a crystalline Hg oxide structure (Table 2). Given the similarity of EXAFS results and XANES spectra for $x = 0.1$ and 0.5 at the lower Hg loadings, that the Hg−S CN is never greater than 1 and that Hg−S coordination remains relatively unchanged with coverage indicate that S−Hg−S bidentate complexes contribute little to the overall Hg coordination structure. Therefore, the results indicate that adsorbed Hg^{2+} forms mostly monodentate sulfur complexes (−S−Hg−OH) with the sulfur functional groups on the MP-HMS surfaces at low Hg loadings.

When the Hg loadings are higher, Hg/S > 0.5, regardless of the sulfur site density or the value of x, the Hg−O path becomes more important with the resulting fits to the data consistent with the formation of a double layer structure of Hg attached to sulfur binding sites (−S−Hg−O−Hg−OH). For these higher coverage data, CN and R increase for Hg−O. The R_{Hg-O} value corresponds more closely to the Hg−O atomic distance of hydrated Hg ion (Table 2) than to the bond distance in a crystalline Hg−O structure. This indicates that adsorbed Hg is forming a double layer with a longer averaged Hg−O distance caused by the second sorbed layer. The increase in Hg−O CN is consistent with second layer of sorbed Hg having two oxygen nearest neighbors. The decrease in Hg−S coordination that accompanies the increased Hg−O distance with coverage can also be attributed to the formation of a −S−Hg−O−Hg−OH double layer surface Hg complex. For instance, for the Hg double layer structure proposed, the average CN of Hg−S should be around 0.5 (one Hg with S while the other Hg without S). The EXAFS results that the CN of Hg−S decreased while R_{Hg-S} remained the same with increasing Hg loading support the formation of Hg double layer.

XAS results from MP-HMS $(SiO_2)_{1-x}(LSiO_{1.5})_x$ with $x = 0.10$ show trends similar to those obtained for $x = 0.50$. This result suggests that the coordination environment of adsorbed Hg changes mostly according to Hg/S loadings rather with than the concentration of sulfur functional groups on the mesoporous surfaces except for the sample with low Hg/S loadings. The data also indicate that the basis for high sorption affinity has to do with the ability of Hg to form strong Hg−S linkages at low loadings. These initially bound mercury centers provide a surface coverage that subsequently serves as an anchor for the formation of surface layers of mixed mercury oxide hydroxide phases at higher loadings.

Acknowledgments

We thank Hoon Young Jeong and Adriano R. Vieira for their help on XAS data collection. Funding for this research was provided by NIEHS Grant P42 ES04911-12. Portions of this research were carried out at the Stanford Synchrotron Radiation Laboratory, a national user facility operated by Stanford University on behalf of the U.S. Department of Energy, Office of Basic Energy Sciences. The SSRL Structural Molecular Biology Program is supported by the Department of Energy, Office of Biological and Environmental Research, and by the National Institutes of Health, National Center for Research Resources, Biomedical Technology Program.

Literature Cited

(1) Huang, C. P.; Blankenship, D. W. *Water Res.* **1984**, *18*, 37−46.
(2) Zamzow, M. J.; Eichbaum, B. R.; Sandgren, K. R.; Shanks, D. E. *Sep. Sci. Technol.* **1990**, *25*, 1555−1569.
(3) Prado, A. G. S.; Arakaki, L. N. H.; Airoldi, C. *Green Chem.* **2002**, *4*, 42−46.
(4) Ghazy, S. E. *Sep. Sci. Technol.* **1995**, *30*, 933−947.
(5) Chiarle, S.; Ratto, M.; Rovatti, M. *Water Res.* **2000**, *34*, 2971−2978.
(6) Dujardin, M. C.; Caze, C.; Vroman, I. *React. Funct. Polym.* **2000**, *43*, 123−132.
(7) Mercier, L.; Detellier, C. *Environ. Sci. Technol.* **1995**, *29*, 1318−1323.
(8) Beck, J. S.; Vartuli, J. C.; Roth, W. J.; Leonowicz, M. E.; Kresge, C. T.; Schmitt, K. D.; Chu, C. T. W.; Olson, D. H.; Sheppard, E. W.; et al. *J. Am. Chem. Soc.* **1992**, *114*, 10834−10843.
(9) Zhao, D.; Feng, J.; Huo, Q.; Melosh, N.; Frederickson, G. H.; Chmelka, B. F.; Stucky, G. D. *Science* **1998**, *279*, 548−552.
(10) Feng, X.; Fryxell, G. E.; Wang, L. Q.; Kim, A. Y.; Liu, J.; Kemner, K. M. *Science* **1997**, *276*, 923−926.
(11) Liu, A. M.; Hidajat, K.; Kawi, S.; Zhao, D. Y. *Chem. Commun.* (*Cambridge*) **2000**, 1145−1146.
(12) Lim, M. H.; Blanford, C. F.; Stein, A. *Chem. Mater.* **1998**, *10*, 467−470.
(13) Mercier, L.; Pinnavaia, T. J. *Chem. Mater.* **2000**, *12*, 188−196.
(14) Mori, Y.; Pinnavaia, T. J. *Chem. Mater.* **2001**, *13*, 2173-2178.
(15) Huggins, F. E.; Huffman, G. P.; Dunham, G. E.; Senior, C. L. *Energy Fuels* **1999**, *13*, 114−121.
(16) Collins, C. R.; Sherman, D. M.; Ragnarsdottir, K. V. *J. Colloid Interface Sci.* **1999**, *219*, 345−350.
(17) Wirnsberger, G.; Pillep, B. M.; Popitsch, A.; Knoll, P.; Behrens, P. *Chemistry—Eur. J.* **2002**, *8*, 3927−3937.
(18) Kim, C. S.; Rytuba, J. J.; Brown, G. E. *J. Colloid Interface Sci.* **2004**, *271*, 1−15.
(19) Kim, C. S.; Rytuba, J. J.; Brown, G. E. *J. Colloid Interface Sci.* **2004**, *270*, 9−20.
(20) Behra, P.; Bonnissel-Gissinger, P.; Alnot, M.; Revel, R.; Ehrhardt, J. J. *Langmuir* **2001**, *17*, 3970−3979.
(21) Xia, K.; Skyllberg, U. L.; Bleam, W. F.; Bloom, P. R.; Nater, E. A.; Helmke, P. A. *Environ. Sci. Technol.* **1999**, *33*, 257−261.
(22) Hesterberg, D.; Chou, J. W.; Hutchison, K. J.; Sayers, D. E. *Environ. Sci. Technol.* **2001**, *35*, 2741−2745.
(23) Bishop, D. B.; McCool, G. D.; Nelson, A. J.; Reynolds, J. G.; Baumann, T. F.; Fox, G. A.; DeWitt, J. G.; Andrews, J. C. *Microchem. J.* **2002**, *71*, 247−254.
(24) Lennie, A. R.; Charnock, J. M.; Pattrick, R. A. D. *Chem. Geol.* **2003**, *199*, 199−207.
(25) Kemner, K. M.; Feng, X.; Liu, J.; Fryxell, G. E.; Wang, L. Q.; Kim, A. Y.; Gong, M.; Mattigod, S. *J. Synchrotron Radiat.* **1999**, *6*, 633−635.
(26) Franson, M. A. M.; Greenberg, A. E.; Trussell, R. R.; Clesceri, L. S. *Standard Methods for the Examination of Water and Wastewater*, 18th ed.; American Public Health Assoc./American Water Works Assoc./Water Pollution Control Federation: Washington, DC, 1992.
(27) George, G. N.; Pickering, I. J.; Stanford Synchrotron Radiation Laboratory, Stanford, CA, 1995.
(28) Ankudinov, A. L.; Ravel, B.; Rehr, J. J.; Conradson, S. D. *Phys. Rev. Part B* **1998**, *58*, 7565−7576.
(29) Brown, G. E., Jr.; Calas, G.; Waychunas, G. A.; Petiau, J. X-ray absorption spectroscopy and its applications in mineralogy and geochemistry. In *Mineral−Water Interface Geochemistry*; Hawthorne, F. C., Ed.; Mineralogical Society of America: Washington, DC, 1988; Vol. 18, pp 431−512.
(30) Wyckoff, Ralph W. G. *Crystal Structures, Vol. 3*, 2nd ed.; Interscience: New York, 1963.
(31) Rodic, D.; Spasojevic, V.; Bajorek, A.; Onnerud, P. *J. Magn. Magn. Mater.* **1996**, *152*, 159−164.

Received for review February 27, 2004. Revised manuscript received June 22, 2004. Accepted July 5, 2004.

ES049689O